Optical properties of ferroelectrics with tetragonal potassium-tungsten-bronze in the fundamental absorption region

Amirulla A. Mamedov

Azerbaïdzhan State University

The reflection spectra of ferroelectrics with the structure of tetragonal potassium-tungsten bronze ($Ba_x Sr_{1-x} O_6$ and $Ba_2 NaNb_5 O_{15}$) are investigated at energies $\hbar\omega = 1.0$ to 35 eV. The results are used to calculate the optical function, to propose an interband-transition energy scheme, and to demonstrate the important role of the NbO_6 octahedron in the formation of the band structure of the crystals.

PACS numbers: 78.20.Dj, 77.80. − e, 71.25.Tn, 71.45.Gm

1. INTRODUCTION

One of the most important and numerous groups of ferroelectrics is the family of oxygen-octahedral crystals. The structure of these crystals is a combination of oxygen octahedra, in the centers and voids of which other ions are located. The family of oxygen-octahedral ferroelectric has three basic structures: 1) perovskite structure, 2) trigonal pseudoilmenite structure, 3) distorted potassium-tungsten bronze structure.

Outstanding representatives of the third group of crystals, diligently investigated in the last few years, are single-crystal solid-solution barium-strontium niobates $Ba_x Sr_{1-x} Nb_2 O_6$ (BSrN) and barium sodium niobate $Ba_2 NaNb_5 O_{15}$ (BSN). The great interest in these compounds is due to their strong optical nonlinearity.[1-3] Further investigations of these compounds have shown them to be promising for purposes of optical reduction of information.[4,5] The interest in these compounds, however, is not restricted to applications only. The presence of the NbO_6 octahedron with different Nb–O bonds in BSrN and BSN and the displacement of the Nb ion in the octahedron in the course of phase transitions lead to changes in many of the macroscopic and microscopic parameters of these crystals. Study of the role of the BO_6 octahedron can cast light on the many physical phenomena that take place in BSrN and BSN. All this has stimulated investigations of the optical properties of BSrN (with barium content $0.25 \leqslant x \leqslant 0.75$) and BSN in a wide spectral range, with an aim at revealing the salient features of the energy spectrum of the electrons and of the character of the interband transitions in them, as well as to determine the role of the BO_6 octahedron in the formation of the band structures of BSrN and BSN. Notice must be taken of the sporadic character of these investigation to date.[6-8] This is due both to procedural difficulties and to the lack of theoretical calculations of the band structure of these compounds. The present investigation is an attempt at a partial filling of these gaps. The results of a study of the optical properties of BSrN and BSN in the range $\hbar\omega = 1.0$–35.0 eV are presented here for the first time ever.

2. EXPERIMENT

1. Processing of crystals

The BSrN and BSN crystals used for our measurements were grown by the Czochralski method and their ferroelectric phase-transition temperatures were $T_c = 840$ K (BSrN) and 320 K $< T_c < 470$ K (BSN) with different barium contents), as determined from dielectric measurements. The BSrN and BSN samples for the investigation of the optical properties were cut from blanks and measured $8 \times 8 \times d$ mm along the crystallographic axes. The crystal thickness (d) ranged from 0.08 to 4.0 mm. The crystals were first mechanically ground and polished, and then bright-dipped (polishing etchant: 40% HF and 70% HNO_3 in a 1:1 ratio). The crystals, ready for optical measurements, were then annealed to remove the elastic stresses. All the optical measurements were made on polished z- and xy-cut faces of single-domain crystals.

2. Measurement technique and experimental procedure

Measurements of optical properties in the vacuum ultraviolet (VUV) region call for special apparatus, of which there are a few published descriptions. We consider it necessary therefore to describe in detail the experimental procedure and the measurement technique used in the investigations. The source of the polarized light was synchrotron radiation from the Stoghton Synchrotron Radiation Center of the University of Wisconsin in Madison (USA). The radiation was fully polarized in the orbit plane. The beam polarization decreased with increasing distance from the orbit plane. The beam from the storage ring was focused on the entrance slit of the monochromator by a system of mirrors. The spectral instrument was a McPherson-225 vacuum monochromator with a 1200 lines/mm diffraction grating. An ion pump produced a vacuum up to 10^{-10} Torr. We have modified the monochromator somewhat to permit automatic rotation (at various speeds) of the diffraction grating and simultaneous reading of the wavelength.
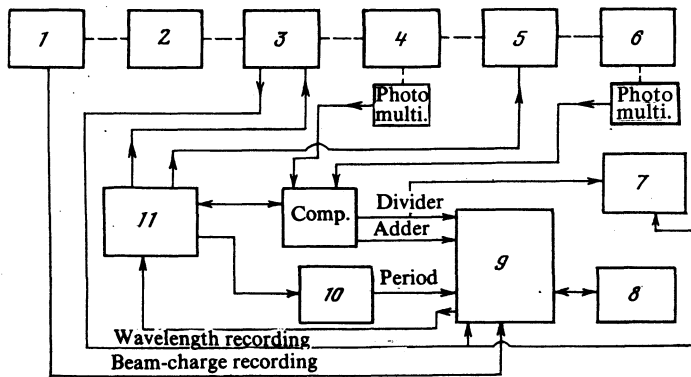
0038-5646/82/111043-07$04.00

FIG. 1. Block diagram of measurement setup (details in text): 1—storage ring, 2—mirror, 3—monochromator, 4—beam splitter, 5—modulator, 6—sample, 7—automatic plotter, 8—teletype, 9—PAP-131 analog-digital converter, 10—time counter, 11—control unit.

A block diagram of the measurement unit for the investigation of the optical properties of solids in the VUV region is shown in Fig. 1. As can be seen from the figure, the monochromatic light passing through the mirror system strikes a beam splitter that performs several functions: (1) delays the scattered light, (2) maintains a high degree of polarization by limiting the beam transmission in the vertical direction, (3) increases the resolving power of the setup. A mechanical chopper placed behind the beam splitter eliminates undesirable noise and decreases the dark currents of the detector. The chamber section in which the sample is located is removable and its construction permits rotation and orientation of the sample. This makes it possible to investigate anisotropic crystals. The radiation detector is a photomultiplier with a phosphorescent window. The detector design is such that its sensitivity to scattered visible radiation is small. The signal from the detector output enters the measurement channel where the data, after selection and storage, are reduced by a digital synchronous computer (DSC). The DSC calculates the signals in the channels (with and without the sample, and their ratios). All the differential quantities were next duplicated on a plotter chart with the aid of an analog-digital converter. A teletype was used to record for each point the wavelength, the electron charge in the storage ring, the summary and differential quantities, and the measurement-cycle time. All these data were simultaneously entered into a computer for further reductions. The measurements in the low-energy region were made with a Perkin-Elmer 301 spectrometer ($\hbar\omega = 0.3$–3.5 eV), with an ordinary incandescent lamp as the light source.

3. Reflection spectra and Karamers-Kronig relation

The spectra of the normal reflection of BSrN single crystals[1] ($x = 0.3$,z-cut) and of BSN single crystals (z-cut) at

room temperature and in the energy range $\hbar\omega = 1.0$–35.0 eV are shown in Figs. 2 and 3. In the energy region $\hbar\omega = 3.0$–12.0 eV these spectra are similar. It can be seen that the R spectra have two broad bands, each with a complex structure (see Table I). In the high-energy region of the spectrum, however, an abrupt decrease of the reflectivity and an absence of structure in the R spectra are observed. At photon energies higher than 15 eV one can see a weak structure in the R spectra of the BSrN and BSN crystals. Lowering the temperature makes the R spectrum more complicated, adds irregularities, and decreases the reflectivity of the crystals.

In addition, we have investigated in greater detail the BSrN and BSN absorption edges for the purpose of elucidating the character of the interband transition, determining the width of the gap width (E_g) and its temperature dependence, and the possible anomalies in the phase transition. Measurements in the low-energy region (< 4 eV) have shown that the absorption edge has an exponential behavior and is subject to a modified Urbach rule. Below 120 K the absorption edge becomes abrupt and indirect optical transitions from phonon participation are observed in experiment. The frequencies of these transitions are in satisfactory agreement with data on Raman scattering of light. On the basis of the obtained data we determined the E_g for indirect transitions at 120 K, namely 3.44 $\pm$ 0.05 eV for BSrN and 3.68 $\pm$ 0.05 eV for BSN, with respective values 5.1×10^{-4} and 4.7×10^{-4} eV/deg for dE_g/dT. Notice should be taken of a property typical of ferroelectrics, namely the absence of anomalies of E_g in the phase-transition region.

To reduce the experimental data and obtain information on the behavior of the optical functions we have used the Kramers-Kronig difference method,[12] which is not very sensitive to the short-wave approximation of the spectrum. For the unmeasured long-wave part of the spectrum R, i.e., for

TABLE I.

| Material	R, eV	ε_2, eV
$Ba_{0.3}Sr_{0.7}Nb_2O_6$ $\hbar\omega_p = 29.5$ eV $\tau_v = 1{,}49 \cdot 10^{-16}$ s	3.18; 3.95; 4.31; 5.07; 5.95; 6.40; 7.82; 9.58; 11.90; 12.43; 13.04; 19.00; 22.05; 23.15; 25.17; 26.00	4.15; 4.55; 5.82; 6.17; 7.39; 7.70; 9.55; 12.33; 18.30; 18.76; 20.34; 21.06; 22.02; 22.69; 22.91; 25.11; 27.05; 28.00
$Ba_2NaNb_5O_{15}$ $\hbar\omega_p = 29.7$ eV $\tau_v = 1{,}45 \cdot 10^{-16}$ s	3.35; 4.72; 5.30; 5.59; 5.90; 6.11; 6.75; 7.33; 8.32; 8.75; 9.57; 10.05; 12.82; 13.55; 14.40; 14.72; 15.10; 15.65; 17.00; 17.70; 18.34; 18.65; 19.23; 19.55; 20.70; 21.48; 22.57; 24.60; 25.00; 25.60; 28.62; 29.25	3.89; 4.51; 4.96; 6.22; 7.28; 8.40; 8.94; 9.51; 9.97; 14.48; 15.60; 17.13; 17.75; 18.20; 18.76; 19.24; 19.75; 21.70; 22.63; 22.98; 23.75; 28.39; 29.30
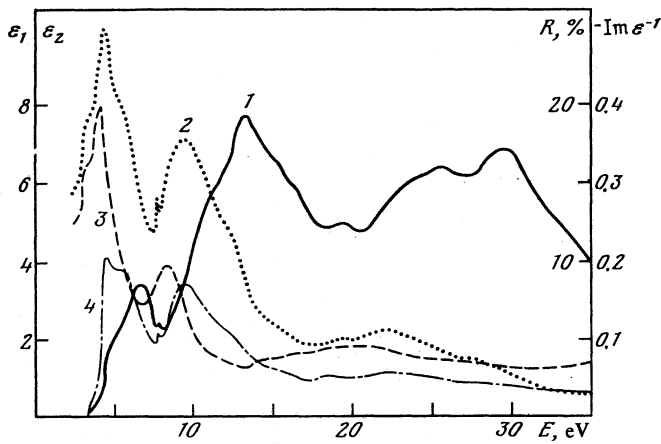
FIG. 2. Spectra of the reflection R (curve 2), of the real and imaginary parts (ε_1 and ε_2, curves 3 and 4) of the dielectric constants, and of the characteristic-loss function ($-\operatorname{Im}\varepsilon^{-1}$, curve 1) of BSrN crystals; $T = 300$ K.

the transparency region, an approximation was made in accord with the single-oscillator dispersion formula

$$n^2(\omega) = 1 + f_0(\omega_0^2 - \omega^2)^{-1}, \tag{1}$$

where f_0 is the oscillator strength and ω_0 is the average frequency corresponding to the self-energy of excitation of the principal oscillator; in the general case these do not differ from the numerical values of the corresponding parameters of the individual atoms.

Under conditions when R is known in the entire measured energy region (and when account is taken of the statements made above), the real (ε_1) and imaginary (ε_2) parts of the dielectric constant are given by

$$\varepsilon_1 = \frac{(1-R)^2 - 4R\sin^2\Phi}{(1+R-2R^{1/2}\cos\Phi)^2}, \quad \varepsilon_2 = \frac{4(1-R)R^{1/2}\sin\Phi}{(1+R-2R^{1/2}\cos\Phi)^2}, \tag{2}$$

where Φ is the wave-reflection phase angle.

The optical functions determined in this manner were calculated with a computer on the basis of the experimental R spectra.
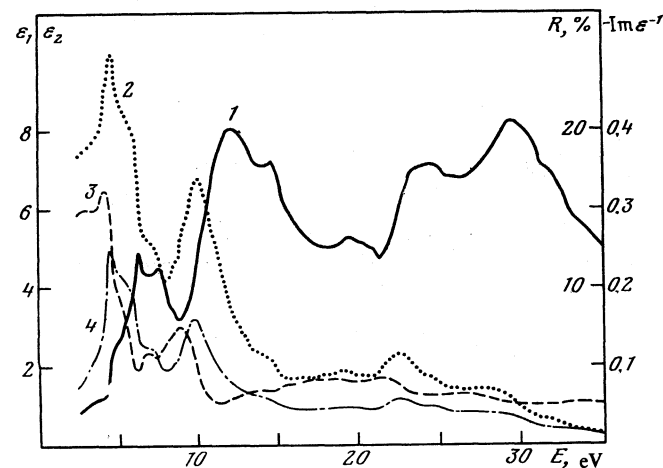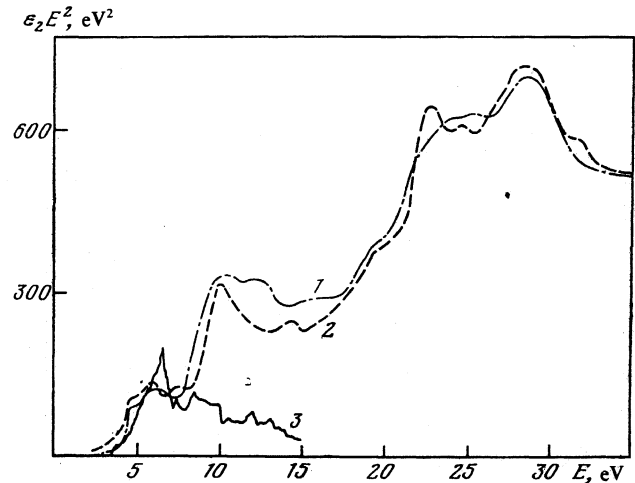

FIG. 3. Same as Fig. 2, but for BSN; $T = 300$ K.

FIG. 4. Spectral distribution $\varepsilon_2(E)^2$ for the crystals BSrN (curve 1) and BSN (curve 2) and histogram (in relative units) for KTaO$_3$ (curve 3).

3. DISCUSSION OF RESULTS

1. Optical functions

Calculation of the phase of the reflected wave and of the optical constants (the refractive and extinction indices) yielded the spectral dependences, shown in Figs. 2–4, of the real (ε_1) and imaginary (ε_2) parts of the dielectric constants and the function, proportional to the combined state density, of the characteristic energy losses ($-\operatorname{Im}\varepsilon^{-1}$) and $\varepsilon_2(\hbar\omega)^2$. The ε_1 and ε_2 spectra correlate well with the R spectra and reach maximum values in the region $\hbar\omega = 5$–12 eV. Notice must be taken of the low values of ε_1 and ε_2 of the investigated crystals, which attest to the high ionicity of BSrN and BSN.

We consider below in greater detail the behavior of one of the most important optical functions.

The spectra $\varepsilon_2(\hbar\omega)$ are complicated in form and are characterized by a structure concentrated in the region $\hbar\omega = 3.0$–12.0 eV (see Figs. 2 and 3). The form of the structure and the shape of ε_2 for the investigated crystals are determined by the positions of the critical state-density points (see Table I). The similarity between the functions ε_2 for BSrN and BSN in the region $\hbar\omega = 3.0$–12.0 eV points to the substantial role and to the fundamental significance of the NbO$_6$ octahedron in the formation of the band structure. This means that the NbO$_6$ octahedron determines the lowest limit of the conduction band and the upper valence band. These bands are similar for many oxygen-octahedral ferrelectrics, since the d-orbitals of the transition metals (of the Nb^{5+} cations) and the p-orbitals of oxygen (of the O^{2-} anions), which are joined in each octahedron, make the main contribution to the bands indicated above. The electronic levels of the oxygen ($2p$) make up the valence band, while the conduction band is made up by the d-orbitals of Nb.

2. Function of characteristic energy losses

At energies lower than 12 eV one observes a decrease of $\varepsilon_2(\hbar\omega)$ and $\varepsilon_1(\hbar\omega)$ (see Figs. 1 and 3) and the absence of an

abrupt structure in the $\varepsilon_2(\hbar\omega)$ spectrum at frequencies higher than the frequency of the transition from the valence to the conduction band. At this frequency the sum of the oscillator strengths for the valence band is spent and the minimum of the $\varepsilon_2(\hbar\omega)$ spectra, observed in a large energy interval, is due to excitation of longitudinal electron oscillations (the so-called plasma oscillations) in the filled valence band. It follows from the foregoing that our measurements of the optical properties in the energy region > 12 eV also yield important information on the character of the interband transitions and on the structure of the valence band and the deeper ones.

The spectra of the function of the characteristic energy losses $-\,\mathrm{Im}\,\varepsilon^{-1} = \varepsilon_2/(\varepsilon_1^2 + \varepsilon_2^2)$ for BSrN and BSN, calculated by us on the basis of the optical measurements, are shown in Figs. 2 and 3. It can be seen from the figures that $-\,\mathrm{Im}\,\varepsilon^{-1}$ is characterized by a complicated spectrum and has maxima both at the energies of the single-particle excitations (~ 6 and ~ 7 eV for BSrN and BSN) and at the plasma-resonance energies (~ 25 eV and ~ 29 eV for BSrN and ~ 25 eV and ~ 29 eV for BSN). It is known that the maxima of $-\,\mathrm{Im}\,\varepsilon^{-1}$ correspond to plasma resonance whenever $\varepsilon_1(\hbar\omega)$ and $\varepsilon_2(\hbar\omega)$ tend to zero in the region of the peak of $-\,\mathrm{Im}\,\varepsilon^{-1}$, and vary linearly with $d\varepsilon_1/d\,(\hbar\omega) > 0$ and $d\varepsilon_2/d\,(\hbar\omega) < 0$ (Ref. 13). This means that the maxima of $-\,\mathrm{Im}\,\varepsilon^{-1}$ in the region below 12 eV are most probably due to the single-particle excitations, since they do not satisfy the conditions for the onset of plasma oscillations. On the other hand, the maxima of $-\,\mathrm{Im}\,\varepsilon^{-1}$ in the region of higher energies correspond to excitation of plasma oscillations of the valence $2p$ electrons of oxygen ($\hbar\omega_1 \approx 25$ eV, $\hbar\omega_2 \approx 29$ eV). It can be seen from the presented $-\,\mathrm{Im}\,\varepsilon^{-1}$ spectra (see Figs. 2 and 3) that the intensities of the high-energy maxima are approximatly equal, with the values of ε_1 and ε_2 tending to zero. All this makes it difficult to determine the energy $\hbar\omega_p$ of the plasma oscillations of the valence electrons from the experimental $-\,\mathrm{Im}\,\varepsilon^{-1}$ curve. To obtain the correct value of $\hbar\omega_p$ we used therefore the known sum rule[14]

$$\int_0^{\omega_0} \omega\,\mathrm{Im}\,\varepsilon^{-1}\,d\omega = -\tfrac{1}{2}\pi\omega_p{}^2. \tag{3}$$

Using (3), we determined from $\hbar\omega_p$ for BSrN and BSN from the energy dependence of $-\,\mathrm{Im}\,\varepsilon^{-1}$ (see Table I). In addition, we determined the relaxation times τ_v that characterize the lifetimes of the plasma oscillations (τ_v^{-1} is proportional to the half-width of the maximum of $-\,\mathrm{Im}\,\varepsilon^{-1}$). The obtained values of τ_v (see Table I) are substantially lower than the relaxation times connected with scattering by the lattice or by an impurity. It can therefore be stated that τ_v is determined by electron-electron scattering. It must be noted that our values of $\hbar\omega_p$ differ from the values calculated by the formula

$$\omega_p{}^2 = \frac{4\pi e^2}{m} N_v, \tag{4}$$

where e and m are the charge and mass of the electron, and N_v is the electron density in the filled valance band.

The values of $\hbar\omega_p$ obtained with the aid of (4) for the six $2p$ electrons in the octahedron, are close to ~ 22 eV. The differences in the numerical values of $\hbar\omega_p$ obtained from optical measurements (see Figs. 2 and 3) using (3) and those calculated from Eq. (4) may be due to the contribution made by the deeper levels owing to the interaction between the valence-band electrons and the atomic-core levels.

3. Atomic-core levels

At photon energies higher than 15 eV the optical functions (R, ε_2) have maxima that can no longer be interpreted as transitions from the valence to the conduction band. We shall therefore attempt to classify the observed transitions on the basis of the data and the earlier experimental data on x-ray photoelectron spectra (XPS).[15] We take from Ref. 15 the experimental data on the atomic-core energy levels O $2s$, Sr $4p$, Ba $5p_{1/2}$, Ba $5p_{3/2}$, as well as the density maxima of the obtained O $2p$ valence states. In a simple atomic analysis, most of the observed transitions can be related to transitions from the atomic-core state into the free Nb $4d$ states, which make up the conduction band. A comparison of our present data with the XPS results allows us to ascribe the transitions into the Nb $4d$ states (in the energy region $\hbar\omega = 15.0$–35.0 eV) to the following atomic-core levels:

(a) In the BSrN case—Ba $5p_{3/2}$ (18.30 eV and 18.76 eV), Ba $5p_{1/2}$ (20.34 eV and 21.06 eV), Sr $4p$ (doublet: 22.02 and 22.69 eV) and O $2s$ 27.05 eV and 28.00 eV);

(b) in the BSN case—Ba $5p_{3/2}$ (14.48 eV, 15.60 eV and 17.13 eV), Ba $5p_{1/2}$ (17.75 eV, 18.20 eV and 19.24 eV), Na $3s$ (22.63 eV and 23.75 eV) and O $2s$ (28.39 eV and 29.30 eV).

To explain the doublet 22.02 and 22.69 eV in the BSrN state we can propose a spin-orbit splitting (Δ) of approximately 0.6 eV for the Sr $4p$ level. The value $\Delta = 0.6$ eV conforms with $\Delta = 0.5$ eV for Sr^{2+} according to Herman and Skillman.[16] It is noteworthy here that since the free states for BSrN and BSN are located in the energy region of the Nb $4d$ levels, the transitions O $2s \to$ Nb $4d$ and Na $3s \to$ Nb $4d$ are dipole-forbidden. This can explain the low intensities of the peaks 27.05, 28.00, 28.35, and 29.30 eV in the data on the reflection and on ε_2. The remaining structures in the R spectra of the BSrN and BSN crystals lie outside this scheme. This is not surprising, since besides the transitions to the Nb $4d$ levels there are transitions into the states Sr $4d$, Ba $5d$ and Nb $5s$, which we are not considering here. In addition, we neglect effects due to electron-hole interactions (e.g., exciton effects), although it is known that they influence strongly the level spectra of the atomic core. From a combination of the energies E_g optically determined from the XPS data and from our results, we can state with assurance that transitions from the atomic-core states into the conduction bands set in at $\hbar\omega \approx 18.0$ eV for BSrN and $\hbar\omega \approx 15.0$ for BSN.

4. Sum rule and effective numbers of valence electron per NbO$_6$ octahedron

From the known sum rules we can determine certain quantitative values, particularly the effective number N_{eff} of the valence electrons and the effective optical dielectric con-
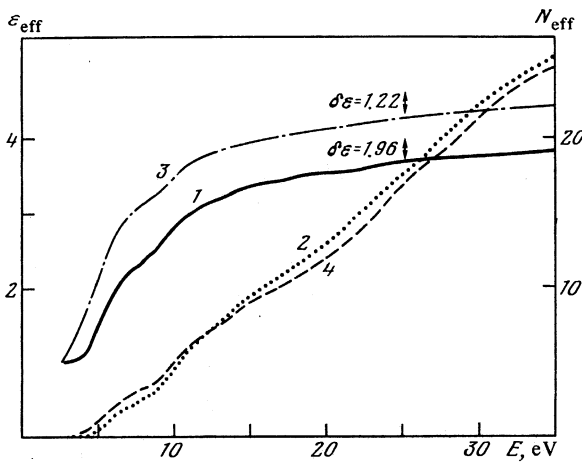
FIG. 5. Spectra of ε_{eff} and N_{eff} of the crystals BSrN (curves 1 and 2 respectively) and BSN (curves 3 and 4 respectively).

stant ε_{eff}, which contribute to the optical constant of the crystal at the frequency ω_0. Recalling that

$$(2\pi N_a e^2/m) N_{\text{eff}} = \int_0^{\omega_0} \omega \varepsilon_2(\omega)\, d\omega,$$

$$\varepsilon_{\text{eff}} = 1 + (2/\pi) \int_0^{\omega_0} \omega^{-1} \varepsilon_2(\omega)\, d\omega \tag{5}$$

(where N_a is the density of the atoms in the crystal), we determine N_{eff} and ε_{eff} from the data obtained by us above.

The physical meaning of ε_{eff} is quite clear[17]: ε_{eff} is the effective optical dielectric constants determined by the interband transitions in the frequency interval from zero to ω_0 (i.e., by the electron-shell polarization). Each of our plots of ε_{eff} vs the incident-photon energy for BSrN and BSN (Fig. 5) can be arbitrarily divided into two parts. The first is characterized by a rapid growth of ε_{eff} and extends to 15 eV. The second part shows a smoother and slower growth of ε_{eff} and tends to saturate at energies above 35 eV.

This means that the largest contribution to ε_{eff} is made by transitions corresponding to the bands at ~ 5 eV and ~ 10 eV (their contribution amounts to $\geqslant 80\%$).

To determine the contribution made to the static dielectric constant $\varepsilon(0)$ by transitions with frequency $\omega > \omega_0$, we compare the maximum ε_{eff} with the square of the refractive index (n^2) measured in the transparency region.[17] The difference $\delta\varepsilon_0 = \varepsilon(0) - \varepsilon_{\text{eff}} > 0$ points to the need for taking into account the polarizability of the deep levels. The obtained difference $\delta\varepsilon_0 = \varepsilon(0) - \varepsilon_{\text{eff}}(\delta\varepsilon_0 = 1.22$ for BSN and $\delta\varepsilon_0 = 1.96$ for BSrN) indicates a large contribution of transitions with $\omega > \omega_0$ to the static dielectric constant.

On the other hand, the N_{eff} determined from the sum rule (5) is the effective number of valence electrons per crystal atom at the energy $\hbar\omega_0$ (under the condition that all the interband transitions possible at this frequency ω_0 were made). In the case of BSrN and BSN the value of N_{eff} (see Fig. 5) increases almost monotonically with increasing photon energy and has no tendency to saturate in the entire investigated energy interval. It is therefore impossible to

choose any independent criteria for the estimate of the number of valence electrons per unit cell. Recognizing that the two conduction subbands $(d\varepsilon, d\gamma)$ are separated from each other and are also separated from the higher-lying states of the conduction band, we can assume a tendency to saturation at energies such that the transitions to the corresponding subbands are exhausted. In other words, since N_{eff} is determined only by the behavior of ε_2 and is the total oscillator strengths, the sections of the $N_{\text{eff}}(\omega)$ curves with the maximum slope, which correspond to the maxima of $dN_{\text{eff}}/d\omega$, can be used to discern the appearance of new absorption mechanisms with increasing energy ($\hbar\omega = 7.0$, 18.0, and 30.0 eV for NSrB and $\hbar\omega = 8.0$, 15.0, and 25.0 eV for NSB). The values of N_{eff} obtained at these energies (assuming the formal ion charges) are smaller than the calculated ones.

5. Band structure

There are at present no calculations of the band structures of BSrN and BSN. We attempt therefore to compare our experimental data in the energy region $\hbar\omega = 3.0$–12.0 eV with the theoretical calculations of the band structure of $SrTiO_3$, a compound from an analogous crystal family.[18,19] According to these references, the highest valence band and the lowest conduction band can be deduced from the wave functions of O^{2-} $(2p)$ and of the Ti^{4+} (Sr^{4+}) free ions. In Ref. 18 the band structure of $SrTiO_3$ was calculated from data on the ionization potentials of the free ions, on the Madelung potentials, and on the electrostatic crystal fields. However, the minimum distance $(E_c - E_v)$ between the valence and conduction bands, calculated in Ref. 18, turned out to be unrealistically large. On the other hand, allowance for the partial covalency of the bands in $SrTiO_3$ improves the calculated data. It was noted in Ref. 19 that this decrease of the distance between the energy levels will be insufficient to obtain the experimentally observed E_g. To reach the observed value of E_g (at the same charge transfer) it is necessary to consider the polarizability of the oxygen anions and the change of the polarization potential as functions of the degree of ionization. What was obtained in fact in Ref. 19 was the value of $E_v - E_c$ near the experimentally observed width of the forbidden band, by subtracting the energy obtained upon polarization of the entire octahedron from the initially obtained value of E_g. Similar results were obtained by Mattheiss,[20] who used other calculation methods and different experimental fit parameters.

Since BSrN and BSN contain the basic BO_6 structure element (as do the perovskites), the main features of the band structure of $SrTiO_3$ (Fig. 6) should be possessed also by these crystals. Of course, since the Nb^{5+} (d), Ba^{2+} (p), and Na^+ (s) wave functions were invoked, certain changes should be observed. This is confirmed by the optical data; just as perovskites, the two basic optical oscillators at 5 eV and 10 eV (see Figs. 2 and 3) correspond to transitions from the valence band to the conduction band made up of d-orbitals of the transition element and consisting of two subbands $(d\varepsilon, d\gamma)$. The presence, however, of other shallower structures in the BSrN and BSN optical spectra at photon energies $\hbar\omega = 3.0$–12.0 eV is attributed by us to distortion of the octahedron
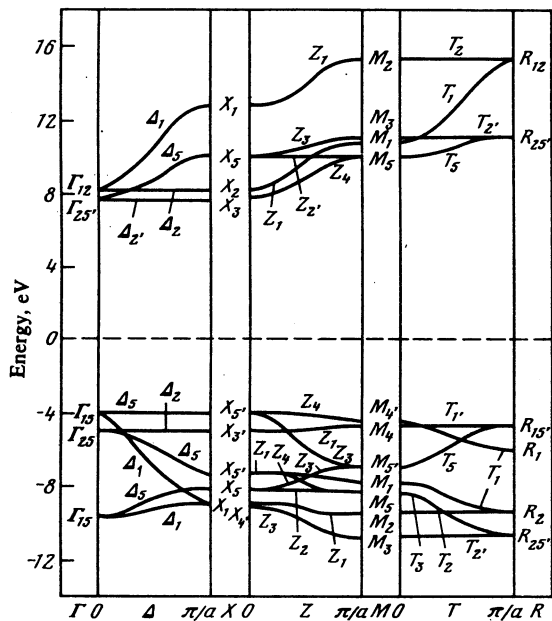
FIG. 6. Band structure of SrTiO$_3$ (Ref. 19).

FIG. 7. Interband transition scheme in BSrN and BSN crystals (VB—valence band, CB—conduction band).

(since the space group changes from O_h^1 (SrTiO$_3$) to C_{2v} BSrN and BSN). This distortion distorts the cubic symmetry much more strongly than the lattice polarization, and weakens the "cubic" selection rules. The tremendous number of overlapping transitions makes it impossible to analyze the line shapes and to relate the experimentally observed interband transitions to definite critical points.

6. Critical points

Assume that, despite the tetragonal distortion, interband transition take place near the cubic-symmetry points[19] Γ, X, and M (see Fig. 6), where the condition $\nabla(E_v - E_c) = 0$ is satisfied in all probability. It can be shown that the highest photon energies should excite electrons into states at the point M ($\geqslant 9$ eV). The principal oscillator would then correspond at 5 eV to transition to the lowest $d\varepsilon$ subbands at X. Theoretical calculations show that the two conduction subbands reflect each other qualitatively, and the same can be said concerning the optical spectra (Figs. 2–7). For example, the shoulder at 4.55 eV is duplicated at 9.55 eV (for BSrN crystals), i.e., in transitions into the band $d\gamma$. In addition, a threefold splitting of the valence band, due to the tetragonal symmetry of the O^{2-} sites, can be observed. We attribute to this the structure 8.94 eV, 9.51 eV and 9.97 eV in the region of the $d\gamma$ transitions for BSN.

We can note that direct transitions start (presumably) at 3.8 and 3.9 eV for BSrN and BSN crystals respectively. Since the absorption is exponential at energies below 3.3 eV (at $T = 300$ K) and is determined more readily by defects, it is impossible to answer this question definitely because of the low absorption coefficients obtained in transmission experiments. If the transitions at 3.8 eV and 3.9 eV are direct, as is predicted by the band calculations, it becomes necessary to explain the unusually small oscillator strengths. As for the high-energy transitions, as shown above (see subsection 3 of
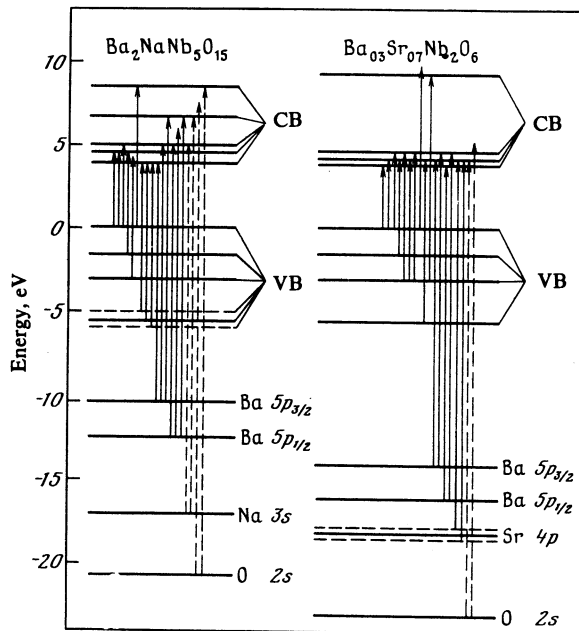
Sec. 3), at photon energies higher than 12 eV the experimental data can differ greatly both relative to SrTiO$_3$ and relative to each other.

We propose on the basis of the experimental data and the presented discussion a simple band model for BSrN and BSN, shown in Fig. 7 and describing the results.

7. State-density function

Plots of $\varepsilon_2(\hbar\omega)^2$ vs $\hbar\omega$ are shown for BSrN and BSN in Fig. 4. These are the most suitable spectra from the viewpoint of experimentally determining the singular points of the state-density function $g(\hbar\omega)$, since $g(\hbar\omega) \sim \varepsilon_2(\hbar\omega)^2$ if it is assumed that the transition matrix elements depend little on the energy. The same figure shows a histogram of the state-density function vs energy for the related oxygen-octahedral crystal KTaO$_3$. A comparison of these curves shows that transitions from the valence band produced by oxygen p-orbitals are realized into two conduction subbands separated by a gap ~ 5 eV. This histogram is one more confirmation of the validity of our assumptions and of the transition energy scheme presented by us for BSrN and BSN.

4. CONCLUSION

The optical properties of single-crystal BSrN and BSN solid solutions, which are typical representatives of oxygen-octahedral ferroelectrics with tetragonal potassium-tungsten-bronze structure, were investigated, using synchrotron radiation, in the energy range 1.0–35.0 eV. The experimental data were used to calculate the spectra of the optical functions and to explain the singularities observed in their spectra. Also determined were important characteristics of BSrN and BSN crystals as E_g and dE_g/dT, the frequency of the plasma oscillations and their relaxation time, and the contribution of the electron-shell polarization to the static

Amirulla A. Mamedov   1048

dielectric constant. The results made it possible to determine the energy transition schemes in the BSrN and BSN crystals and to confirm the basic role of the BO_6 cluster in the formation of the band structure of these compounds.

In conclusion, the author considers it his pleasant duty to thank E. M. Rowe, D. W. Lynch, and F. Ullman for collaboration and help with the experiment, C. G. Olson for help with the measurement, the University of Nebraska and the Ames Laboratory of the USA Atomic Energy Commission for subsidizing the experiment, G. A. Smolenskiĭ, R. Braunstein, V. Ren, and A. Kh. Zeĭnally for a discussion, a fruitful discussion, and valuable remarks.

---

[1] The spectra of BSrN single crystals with barium contents $0.25 < x < 0.75$ differ little in the investigated region.

[1] A. K. Chakravati and U. P. Phadke, J. Appl. Phys. **45**, 1461 (1974).

[2] R. L. Byer, S. E. Harris, D. J. Huizenga, J. F. Fong, and R. S. Feigelson, J. Appl. Phys. **40**, 444 (1969).

[3] L. M. Dorozhkin *et al.*, Kvant. Elektron. (Moscow) **4**, 2266 (1977) [Sov. J. Quantum Electron. **7**, 1298 (1977)].

[4] N. N. Lebedeva, A. M. Mamedov, and A. H. Zejnally, Ferroelectrics **31**, (3/4), 117 (1981).

[5] J. B. Thaxter, "NEREM" Record, Boston, Vol. 11, p. 10 (1969).

[6] N. N. Lebedeva and A. M. Mamedov, Bull. Am. Phys. Soc. **24**, 508 (1979).

[7] M. Cardona, Phys. Rev. **140**, 651 (1965).

[8] N. N. Lebedeva, A. M. Mamedov, and N. N. Svistunova, Fiz. Tverd. Tela (Leningrad) **23**, 594 (1981) [Sov. Phys. Solid State **23**, 335 (1981)].

[10] L. C. Bobb, I. Lefkowitz, and L. Muldawer, Ferroelectrics **2**, 217 (1971).

[11] V. M. Fradkin, Segnetoélektriki-poluprovodniki (Ferroelectrics-Semiconductors), Nauka, 1975.

[12] R. K. Ahrenkie, J. Opt. Soc. Amer. **61**, 1651 (1971).

[13] H. Philipp and H. Ehrenreich, Phys. Rev. **129**, 1550 (1963).

[15] F. L. Battye, H. Hochst, and A. Goldmann, Sol. St. Commun. **19**, 269 (1976).

[16] F. Herman and S. Skillman, Atomic Structure Calculations, Prentice Hall, 1963.

[17] A. I. Galuza and A. P. Kirichenko, Ukr. Fiz. Zh. **26**, 1083 (1981).

[18] A. H. Kahn and A. J. Lyendecker, Phys. Rev. **135**, A1321 (1964).

[19] T. F. Soules, E. J. Kelly, D. M. Waught, and J. W. Richardson, Phys. Rev. **B6**, 1519 (1972).

[20] L. F. Mattheiss, Phys. Rev. **B6**, 4718 (1972).